JTTEE5 17:456–464
DOI: 10.1007/s11666-008-9202-4
1059-9630/$19.00 © ASM International

Efficiency of Pulsed Detonation Thermal Spraying

Jacob E. Cannon, Mohammad Alkam, and P. Barry Butler

(Submitted December 2, 2007; Accepted April 16, 2008)

Pulsed detonation thermal spray coating is used to enhance the material properties at the surface of an object. The present research implements computational fluid dynamic modeling to identify the efficiency of energy and mass delivered to potential target locations. Six cases of a hydrogen-air mixture are used to investigate the gas flow from the instant of ignition to the instant of flow reversal at the tube exit. Flow monitors are included in the model to represent potential target locations. These monitors are placed at different axial locations in order to record mass flow rate and the flow rate of enthalpy over time. The results indicate that there exists a quasi-steady jet that is efficient and predictable in delivery of energy and mass from the tube exit to potential target locations positioned on the centerline. The duration of the quasi-steady jet is dependent on the fraction of combustible gas (i.e., % fill). Much of the initial energy and mass delivered from the jet avoids the flow monitors. This is found to be related to the evolution of the jet behind the blast wave where energy is lost in expansion and vorticity production. It is also found that nearly 11-18% of the available energy and 20-23% of the available mass remains in the tube after flow reversal.

Keywords premixed flame, pulsed detonation, spray coating, thermal spray

1. Introduction

In a pulse detonation thermal spray (PDTS) device, powdered metal alloys and ceramics are delivered to the face of substrate materials by the use of highly energetic carrier gases. The energy (thermal and kinetic) imparted to the powder forces individual particles into the structure of the substrate, thus modifying the properties at the surface. The powder materials are chosen such that they give an apparent surface hardness that is higher than the substrate hardness. This is a desirable property for parts exposed to stressful environments over long periods of time. The powder can also be applied to avoid secondary machining operations for tight tolerances that may be required of the final product.

As with most operations, there are many parameters involved in the successful use of PDTS devices for coating. Porosity, uniformity, and oxidation level are some of the major considerations which are affected by the powder properties and by the manner in which the powder is deposited on the substrate. The production of the fine powder can be difficult to control. Lot-to-lot variations of the powder are known to be an issue (Ref 1). The methods in which the powder is transferred onto the substrate have been a topic of much research. Processes such as plasma spraying, high velocity oxygen fuel spraying, PDTS, and cold gas spraying have all been used in industry. No matter the process, they all have the goal to ensure the incident powder coats the target in such a way that the desirable properties of the final part are achieved. There exist many modes of transporting the particle to the substrate as it traverses in time, position, and undergoes phase changes. The oxidation exposure of a particle that changes from solid to molten prior to impact is a concern that is directly related to how the particle arrives at the substrate. Cold gas spraying has been recently introduced and addresses the oxidation issue (Ref 2). The powder in cold gas spraying is given sufficient velocity that it adheres to the substrate upon impact through plastic deformation, thus avoiding the need to partially melt the particle prior to impact (Ref 3).

The present research is concerned with the PDTS process used to adhere fine particles onto a substrate. Figure 1 illustrates the key components of a simplified PDTS device midway through a single cycle. At the start of a firing cycle, the PDTS tube is filled with gaseous reactants and spark initiated at the breach end. Because of the confined geometry at the ignition point (i.e., breach end), an accelerating combustion wave starts propagating through the unburnt reactants. Under well-characterized fuel/oxidizer initial conditions, the subsonic combustion wave transitions to a supersonic detonation a short distance from the ignition point. Combustion products that form behind the detonation wave simultaneously propel the injected powder toward the exit end and heat the particles. For most reactant mixtures used in PDTS devices, the speed of the detonation wave is on the order of 1000-2500 m/s, and the combustion products behind the

Jacob E. Cannon and **P. Barry Butler**, Department of Mechanical and Industrial Engineering, The University of Iowa, Iowa City, IA 52242; and **Mohammad Alkam**, Department of Mechanical Engineering, Jordan University of Science and Technology, Irbid, Jordan. Contact e-mail: Patrick-butler@uiowa.edu.

Nomenclature

a	speed of sound (m/s)
A_f	pre-exponential factor (m^3/kmol s) used in the Arrhenius expression
D	tube diameter (m)
e	specific internal energy (J/kg) (thermal or sensible only)
E	activation energy (J/kmol) used in the Arrhenius expression
$\vec{F}(\vec{U})$	flux vector in the axial direction
$\vec{G}(\vec{U})$	flux vector in the radial direction
$h^o_{f,i}$	enthalpy of formation of species i at standard state (1atm, 298.15k) (J/kmol)
$\dot{H}$	flow rate of sensible enthalpy (kJ/s)
$\vec{J}(\vec{U})$	source vector
k_f	forward reaction rate
k_b	backward reaction rate
$K(T)_{eq}$	equilibrium constant
L	tube length (m)
m	mass (kg); with overdot signifies per unit time
$M_{w,i}$	molecular weight of species i (kg/kmol)
p	pressure (Pa)
r	tube radius (m) or position or displacement in radial direction of cylindrical coordinate system (m)
R_U	universal gas constant (J/kg·K)
t	time from an initial event or time from blast exiting the tube (s)
T	temperature (K)
u	velocity component in the axial direction (m/s)
v_x	velocity in the axial direction, cylindrical coordinates (m/s)
v_r	velocity in the radial direction, cylindrical coordinates (m/s)
V	velocity (m/s)
Y_i	mass fraction of species i
$\vec{U}$	solution vector
x	position or displacement in axial direction of cylindrical coordinate system (m)

Greek Symbols

β	temperature exponent in the Arrhenius expression
ρ	density (kg/m^3)
$\dot{\omega}_i$	rate of production (or destruction) of the species i (kmol/s m^3)
Δ	difference between final and initial states

Subscripts and Superscripts

1	state ahead of disturbance, downstream or low pressure region in shock tube
4	high pressure region in shock tube
e	exit
o	standard state (1 atm)
i	species, or inlet

Abbreviations

atm	atmosphere
AUSM+	Advection Upstream Splitting Method
CJ	Chapman-Jouguet
CFD	computational fluid dynamics
CFL	the Courant-Friedrichs-Lewy stability condition
D1	exterior flow monitor $x = 1$D from tube exit, centered on the centerline
D2	exterior flow monitor $x = 2$D from tube exit, centered on the centerline
D3	exterior flow monitor $x = 3$D from tube exit, centered on the centerline
TVD	total variation diminishing, referring to a numerical method in CFD

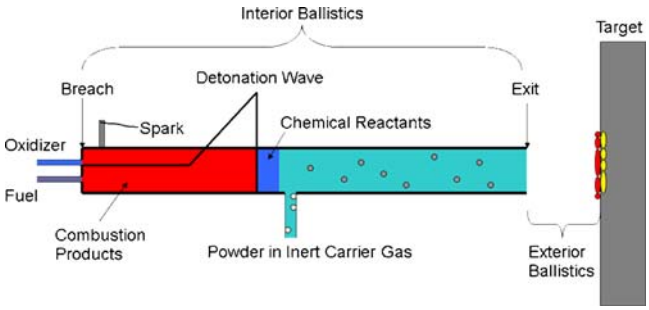

Fig. 1 Illustration of key components of PDTS device

detonation wave move at speeds of 400-800 m/s. The powder speed depends on a number of factors including size, shape, injection location, and tube length. For the purpose of this study, we will neglect the powder, and focus exclusively on what is referred to as the ''exterior ballistics,'' i.e., the flow features outside the PDTS tube. It will be demonstrated that the exterior ballistics plays a key role in a PDTS's efficiency of delivery on the target. System geometry and fuel composition are found to be important in this process (Ref 4). Flow rate of the carrier gas, spray distance, and the fuel/oxygen ratio are significant parameters identified from a Taguchi statistical evaluation based on experiments (Ref 5). Saravanan et al. (Ref 5) found that spray distance is the most important parameter for hardness, and carrier gas flow rate is the most important parameter for porosity.

The objective of this research is to investigate the energy and mass efficiency of the pulsed detonation process. This is accomplished by studying the fraction of mass and energy delivered from a detonation tube that reaches potential target locations and by comparing cycle times. Because a PDTS device is characterized by the supersonic expansion of high-pressure carrier gas at the

exit of an open tube, it is known a priori that a fraction of the gas (and powder) diverges from the centerline upon exiting the tube. By using computational ''flow monitors'' at various axial distances downstream of the exit plane, it is possible to characterize both thermal and mass efficiencies of a PDTS device under various operating conditions.

2. Problem Description

The present research will focus on a single pulse of a PDTS device without powder. A single cycle process is defined as the time the gas is ignited at the closed end of the tube (the breach) to the time that the flow reverses at the tube exit. This research investigates six cases where 0.5 m long tubes of 10 mm and 20 mm diameters are filled with three different amounts of a hydrogen-air mixture. The hydrogen amount in the mixture is chosen as 15.9 vol.% which is close to the theoretical lean limit of detonability. The data for hydrogen-air mixtures in the literature are quite extensive and allows for accurate modeling of the detonation wave. During the wave travel, gas flow is monitored inside and outside the detonation tube. Results for this research are obtained by solving the axisymmetric, compressible, reactive Euler equations. Time histories of mass flow rate, the flow rate of enthalpy, and pressure are gathered throughout the process. Energy and mass delivery to potential target locations are investigated. The times taken for pressure at the breach to reach below 1 atm and for flow reversal (i.e., inflow) at the tube exit are compared between cases.

3. Mathematical Model

In this research, a two-dimensional axisymmetric model is implemented since it is known to model circular jets well (Ref 6). The coordinate system is represented as (x, r) where x is the axial coordinate and r is the radial coordinate.

The governing equations can be written in a column vector form as:

$$\frac{\partial \vec{U}}{\partial t}+\frac{\partial \vec{F}(\vec{U})}{\partial x}+\frac{\partial \vec{G}(\vec{U})}{\partial r}=\vec{J}(\vec{U}) \qquad \text{(Eq 1)}$$

The first vector in Eq 1 is the solution vector and contains dependent variables. $\vec{F}(\vec{U})$ and $\vec{G}(\vec{U})$ are the flux vectors and $\vec{J}(\vec{U})$ is the source term.

$$\vec{U}=\begin{bmatrix}\rho\\ \rho v_x\\ \rho v_r\\ \rho\left(e+\frac{V^2}{2}\right)\\ \rho Y_i\end{bmatrix} \qquad \text{(Eq 2)}$$

$$\vec{F}(\vec{U})=\begin{bmatrix}\rho v_x\\ \rho v_x^2+p\\ \rho v_x v_r\\ \left(\rho\left(e+\frac{V^2}{2}\right)+p\right)v_x\\ \rho Y_i v_x\end{bmatrix},\quad \vec{G}(\vec{U})=\begin{bmatrix}\rho v_r\\ \rho v_r v_x\\ \rho v_r^2+p\\ \left(\rho\left(e+\frac{V^2}{2}\right)+p\right)v_r\\ \rho Y_i v_r\end{bmatrix} \qquad \text{(Eq 3)}$$

$$\vec{J}(\vec{U})=\begin{bmatrix}\frac{-\rho v_r}{r}\\ \frac{-\rho v_r v_x}{r}\\ \frac{-\rho v_r^2}{r}\\ -\left[\left(\rho\left(e+\frac{V^2}{2}\right)+p\right)\frac{v_r}{r}\right]-\sum_i h_{f,i}^{o}\dot{\omega}_i\\ -\frac{\rho Y_i v_r}{r}+\dot{\omega}_i M_{w,i}\end{bmatrix} \qquad \text{(Eq 4)}$$

In the present investigation, all gases are assumed to be ideal with temperature-dependent specific heats. Chemical kinetics is modeled by a 1-step global reversible equation for a hydrogen-air mixture as (Ref 7, 8):

$$H_2+\frac{1}{2}O_2 \Leftrightarrow H_2O \qquad \text{(Eq 5)}$$

N_2 is present in the model, but is inert and does not participate in the reaction. The rate equations for the present reaction step are:

$$\frac{-dC_{H_2}}{dt}=\frac{-2dC_{O_2}}{dt}=\frac{dC_{H_2O}}{dt}=k_f C_{H_2}^1 C_{O_2}^1-k_b C_{H_2O}^1 \qquad \text{(Eq 6)}$$

where $(dC_i/dt)=\dot{\omega}_i$ is the molar production rate of species i. The forward rate k_f is found using the Arrhenius expression for the reaction rate.

$$k_f=A_f T^{\beta} e^{-E/R_u T} \qquad \text{(Eq 7)}$$

where A_f is the pre-exponential factor and is in units of (m^3/kmol s), β is the temperature exponent, E is the activation energy in J/kmol, R_u is the universal gas constant, and T is the temperature in Kelvin. The backward rate k_b is found from the definition of the equilibrium constant.

$$k_b=\frac{k_f}{K(T)_{eq}} \qquad \text{(Eq 8)}$$

4. Computational Model

The present calculations have been carried out using Fluent 6.3. Following is a description of the solution domain and the code setup.

4.1 Solution Domain and Grid Size

Ramadan (Ref 4) demonstrated that a 0.5-mm grid size inside the tube gives accurate results for predicting states of interest in a similar type of application (i.e., shock front exiting a PDTS tube). Ramadan (Ref 4) successfully used a 1.25-mm square grid for the exterior. Ishii et al. (Ref 6) showed that a two-dimensional square grid of 0.5 mm can handle the jet features exiting the tube. In the present calculations, a 0.5-mm grid size has been adopted. Since the current domain is considered axisymmetric, the upper half of the axisymmetric solution domain is shown in Fig. 2. The legend refers to the boundary conditions in the domain. All walls (*solid lines*) are assumed to be adiabatic and impermeable. The interior boundaries (*light dashed lines*) are used to help define regions and monitors in the flow. These interior boundaries are completely passive and do not influence the flow.

Ishii et al. (Ref 6) explained that the downstream boundary can have significant effects on the jet flow and must be sufficiently far away. Ishii et al. (Ref 6) have chosen an axial distance of 15 times the tube radius for the domain in which jets up to $t = 1$ ms duration were studied. The location of the top wall is less important since at that location the reflected waves will be weaker. Ramadan (Ref 4) explained that the wave decays in the radial direction as it exits the tube. Ishii et al. (Ref 6) chose a ratio of about 1.8:1 for the downstream-to-top boundary condition. In the Ishii et al. (Ref 6) study, the highest tube exit-to-reservoir pressure ratio is 5, the time of interest from the blast exit is $t = 1$ ms, and the flow is studied about $x = 80$ mm from the tube exit. In this research, the highest exit-to-reservoir pressure ratio is about 11, the time of interest from blast exit is just under $t = 2$ ms, and the flow of interest is out to $x = 60$ mm from the tube exit. Therefore, the top and right wall boundaries are set 25 and 45 times the largest tube radius, respectively. These far boundary conditions are over three times the size of the Ishii et al. (Ref 6) dimensions. This gives approximately 1.8:1 for the downstream-to-top boundary ratio and allows the jet to be studied for $t \geq 1$ ms without concern for reflective waves.

Estimating that the initial blast wave coming out of the tube is weak after propagating a few diameters from the tube exit, it is approximated that the blast disturbance moves on the order of the speed of sound of the reservoir gas. In fact, the blast wave is known to approach the sonic velocity asymptotically (Ref 6). This assumption implies the wave would take approximately 1.3 ms to reach the downstream boundary and approximately $t = 0.7$ ms to reach the top boundary after it exits the tube. It is expected that the reflection of the wave from the top boundary will be near the end of the jet duration at around $t = 1.4$ ms, and the effects are estimated as small when compared to the flow in the jet.

4.2 Solution Algorithm

As mentioned earlier, a two-dimensional axisymmetric model has been used. The Fluent 6.3 two-dimensional, axisymmetric, double-precision, density based, parallel solver is employed throughout this research. The density-based solver uses the continuity equation to find the density, and the pressure is found from the equation of state. This approach solves all the governing equations at the same time (i.e., coupled), to include species transport. The density-based solver is used with a coupled-explicit formulation that linearizes the governing equations in order to solve a single unknown in each equation. This system of equations is solved simultaneously in each cell at a time. The linearization procedure uses existing values to ensure one unknown variable is present in every equation.

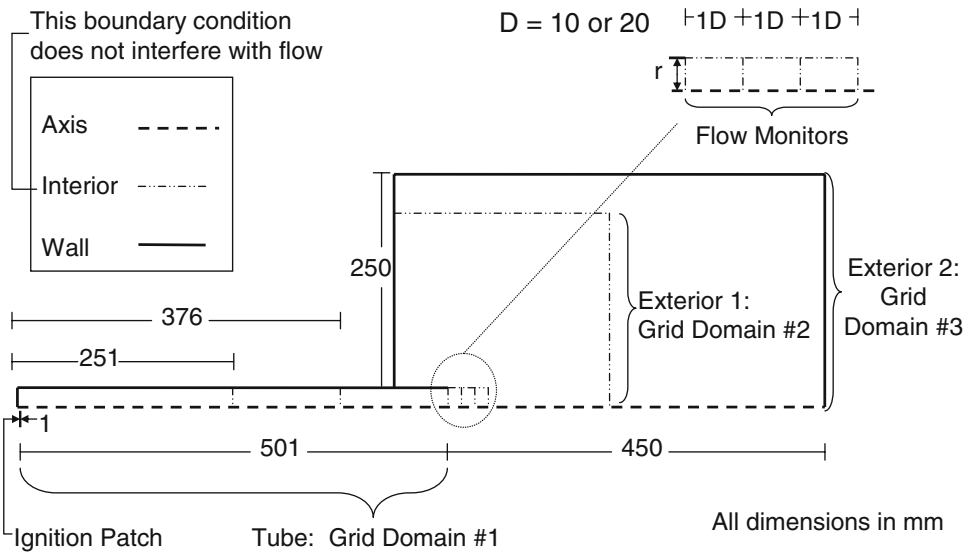

Fig. 2 Present solution domain

Fluent employs a multi-stage Runge-Kutta solver for updating the solution.

A second-order accurate upwind scheme has been used for the spatial discretization. The values of the convected flux at the faces of the control volume are approximated from the cell centroid. The gradient of the scalars in each cell is needed in order to estimate the value at the cell face. A least square cell-based gradient evaluation is used to approximate this gradient. Anderson (Ref 9) pointed out that upwind schemes are designed to simulate the direction of the information moving along the characteristic curve. Anderson (Ref 9) also pointed out that if upwinding was properly implemented, it could handle discontinuities such as shocks within only two grid points. The Courant-Friedrichs-Lewy (CFL) condition has been used to find the time step size

$$\Delta t = \frac{\mathrm{CFL} \cdot \Delta x}{(u + a)_{\max}} \qquad \text{(Eq 9)}$$

where Δx is the grid size and the denominator is the slope of the characteristic line, the maximum local eigenvalue of the characteristic matrix in the axial direction. Each explicit time step is global utilizing a 4-stage Runge-Kutta scheme.

The time step is chosen by the knowledge of the speed of the flow, consideration of the finite rate chemistry, and trial and error. The detonation velocity known from literature and equilibrium codes of the mixture of interest (15.9% volume of hydrogen in air) is known to be 1564 m/s (Ref 10). The 0.5-mm grid size is known to work well in finding the Chapman-Jouguet (CJ) point since the reaction zone is known to be on the order of 5 mm (Ref 11). The 0.5-mm grid size gives about 10 cells in the reaction zone. Since the CFL needs to be less than or equal to unity for convergence a good estimation might be:

$$\Delta t = \frac{0.0005\ \mathrm{m} * 1}{1564\ \mathrm{m/s}} = 3.2 \times 10^{-7}\ \mathrm{s} \qquad \text{(Eq 10)}$$

However, this time step proves too large for capturing the finite rate chemistry in the tube. It is found that a time step on the order of 10^{-8} s works well for capturing the CJ condition; therefore, the CFL of 0.05 has been chosen. This ensures the Damkohler number stays near unity (Ref 11).

The flux vectors are computed using the Advection Upstream Splitting Method (AUSM+) scheme. This scheme utilizes characteristic speeds from surrounding cells in order to compute the Mach number at the cell face (Ref 12). The computed Mach number is used to find the upwind extrapolation of the convected values. The scheme can be free from oscillations when solving shocks, doing so without adding artificial dissipation.

Liou (Ref 13) demonstrated the comparable accuracy of the AUSM+ in a common shock tube scenario (Sod's problem) by comparing it directly to the widely used Roe flux splitting scheme. However, some of the problems in this research deal with pressure and density ratios greater than those in the Sod problem. Therefore, it is important to note that Liou (Ref 13) demonstrated the AUSM+ to be free from oscillations in a case of higher pressure and density ratios, whereas the Roe scheme is not. Dumbser et al. (Ref 14) comment that the AUSM+ method produces only weak shock instabilities when compared to the original Roe scheme. These oscillations are well known in the literature and are addressed in the Fluent 6.3 solver with the introduction of the AUSM+ scheme by Liou and Steffen (Ref 12). Quirk (Ref 15) refers to these spurious solutions generated from solving shocks with the Euler equations as being part of "The Great Riemann Solver Debate." Quirk (Ref 15) pointed out that every Riemann solver has its shortcomings and that perhaps such solvers should be combined with a "complimentary solver" in order to dynamically select the best upwinding for the local flow. Quirk (Ref 15) also pointed out that many of these problems could be solved with artificial dissipation, but this technique is not favored because it reduces the accuracy of the solution. For this reason, slope limiters were not used in the present research.

A shock tube problem has been chosen in this research to validate the ability to handle shocks within the detonation tube. The initial conditions of the shock tube have been chosen such that the resulting incident shock is on the order of the theoretical CJ conditions (Ref 10). It has been found from this problem that the Roe flux difference splitting exhibited oscillations near the shocks when the 0.5-mm square grid is used with second-order accurate upwinding. It is also confirmed that the AUSM+ scheme does not exhibit the oscillations and that it is comparable to the Roe scheme in all other regions. Therefore, the AUSM+ scheme is chosen over the Roe scheme.

4.3 Model Validation

In order to validate the present model, the sonic underexpanded flow problem has been solved. Present results have been compared to the literature. The expansion of the exhaust gases in a PDTS device produces unsteady circular jets. Ishii et al. (Ref 6) conducted a series of experiments that were matched with numerical models for unsteady circular jets resulting from exhausting a $D = 20$ mm diameter shock tube into a quiescent reservoir. They solved the Euler equations for axisymmetric flow by a finite difference TVD scheme proposed by Chakravarthy and Osher (Ref 16). The exterior computational domain size used in this validation matches the exterior computational domain used by Ishii et al. (Ref 6). However, in Ref 6, they used an inlet boundary condition to exhaust the gas into the exterior, whereas this validation simulates the actual shock tube used in the experiment. Ishii et al. (Ref 6) used a 0.25-mm square grid and the present validation study used a 0.5-mm square grid in order to be consistent with the grid used in the present work.

A monitor was placed at the shock tube exit in order to monitor the pressure-time history for the $p_4/p_1 = 8.7$ case. The results of this pressure history are presented in Fig. 3 and match well with Ishii et al. (Ref 6) data.

Figure 4 compares the density results of Ishii et al. (Ref 6) with the present study at $t = 156$ μs. The top of Fig. 4 is a plot of unfilled density contours from the numerical simulation in this research and is compared with the photographs of the actual jet in the bottom portion of Fig. 4.

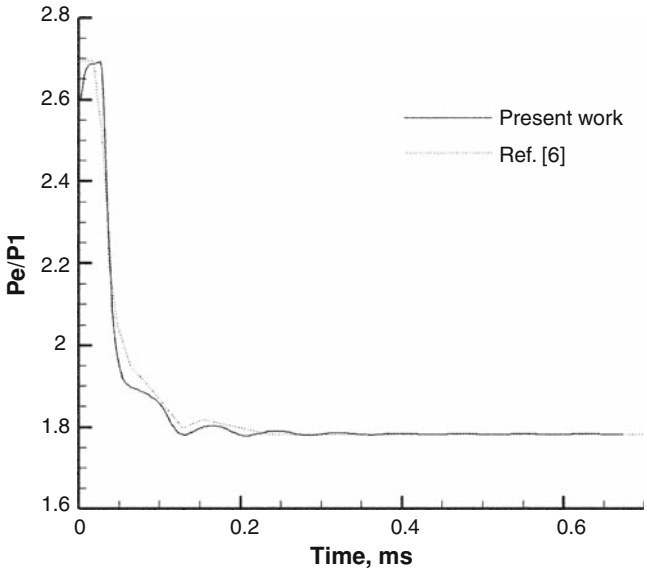

Fig. 3 Normalized centerline tube exit pressure from present study

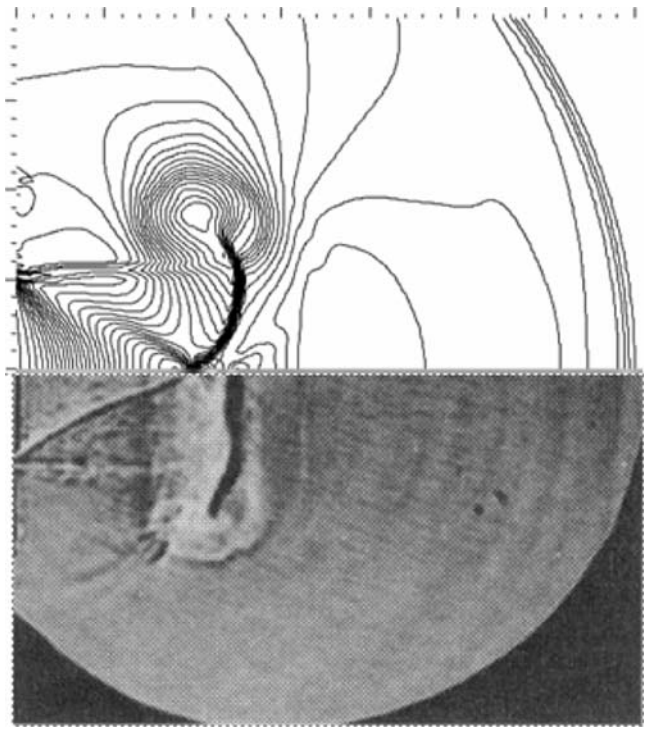

Fig. 4 Present density contours for $p_4/p_1 = 8.7$ at $t = 156$ μs. Compare the top (present model) and bottom (Ref 6) portion

5. Discussion of Results

The results presented in this section focus on filled or partially filled detonation tubes of $L = 0.5$ m with two different diameters, $D = 10$ mm and $D = 20$ mm. A total of six cases were solved from the time of direct detonation at the breach (closed) end of the tube to the instant of flow reversal at the tube exit. Initial conditions for the cases are summarized in Table 1.

For each case, the filled zone of the tube has an initial mixture that consists of a hydrogen-air mixture with a 15.9% hydrogen on volume basis. The initial pressure and temperature are $p = 1$ atm and $T = 300$ K, respectively. The rest of the domain contains pure nitrogen at $p = 1$ atm and $T = 300$ K. More details on the initial conditions and material properties can be found in Ref 17. The chosen initial concentration of hydrogen is close to 15.8%, the theoretical lean limit of detonability for % H_2 (by volume) (Ref 18). The initial conditions are also chosen because there is excellent experimental data available to model the laminar finite-rate chemistry in this research (Ref 7, 8).

As depicted in Fig. 2, exterior flow monitors are placed at locations 1, 2, and 3 diameters downstream of the tube exit. There is also a flow monitor placed at the tube exit plane. A flow monitor is a numerical interior boundary used to track the flow across a particular location in the flow field. It does not influence the flow. The diameters of the monitors are the same diameter used for the tube exit. The flow variables $\dot{m}$ (kg/s) and $\dot{H}$ (kJ/s) through these monitors are written from the time the leading shock exits the tube ($t = 0$ at blast exit) until flow is reversed at the tube exit. The flow variables $\dot{m}$ (kg/s) and $\dot{H}$ (kJ/s) are also recorded at the tube exit plane.

Figure 5 depicts density contours for Case 4, 400 μs after the blast front has exited the tube. The figure shows the main features of the flow. The blue region resembles the jet outside the tube. The blast wave leads the jet significantly. Reflected shocks can be seen off of the left wall. The enlarged portion of the figure illustrates the complex flow structure resulting from the expansion of the high-pressure product gases from the PDTS device.

Rates of energy and mass delivered by the flow at the flow monitor locations have been calculated. Figure 6 and 7 show the flow rates of enthalpy and mass, respectively, at the exit plane for cases 4-6. The integral under each curve represents the maximum mass or enthalpy available for a single cycle for the given conditions. These figures also show that there exists an initial spike in outflow followed

Table 1 Cases defined

Case	*D*, m	*L*, m	% Volume filled with fuel mixture
1	0.01	0.5	100
2	0.01	0.5	75
3	0.01	0.5	50
4	0.02	0.5	100
5	0.02	0.5	75
6	0.02	0.5	50

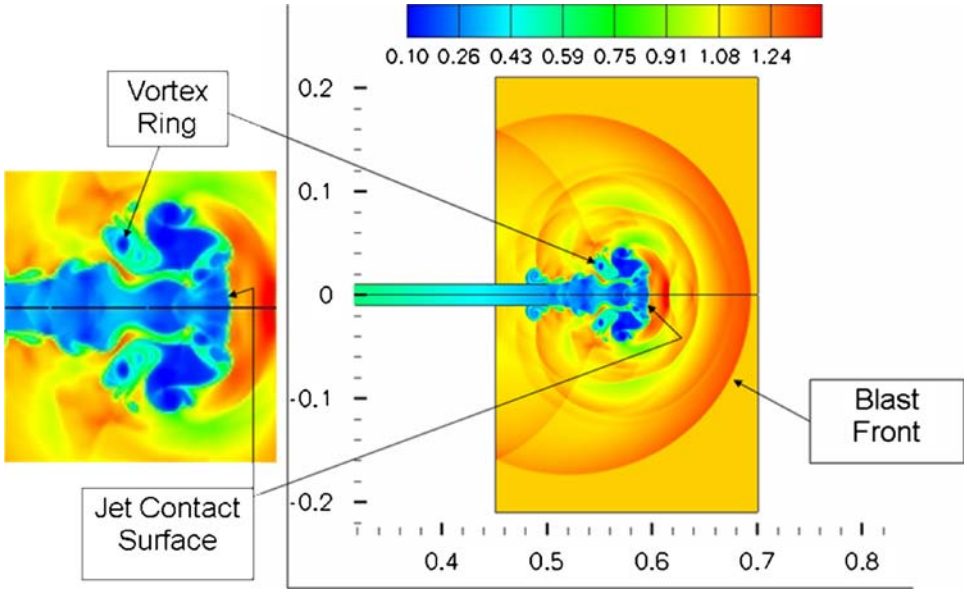

Fig. 5 Density (kg/m^3) contours at $t = 400$ μs after blast exit. Case 4

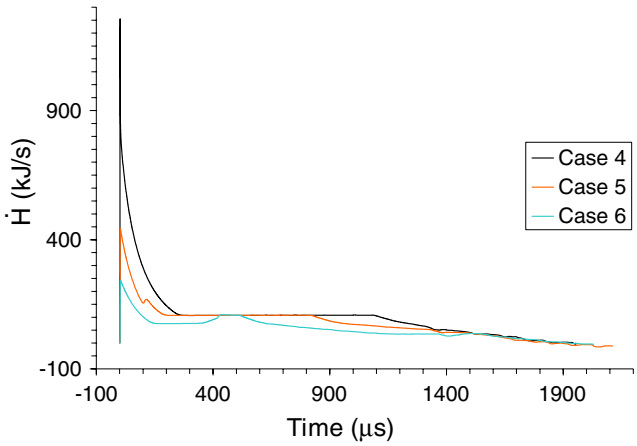

Fig. 6 Flow rate of enthalpy (kJ/s) through the tube exit plane. $t = 0$ corresponds to the time at which the blast exits the tube. Cases 4–6

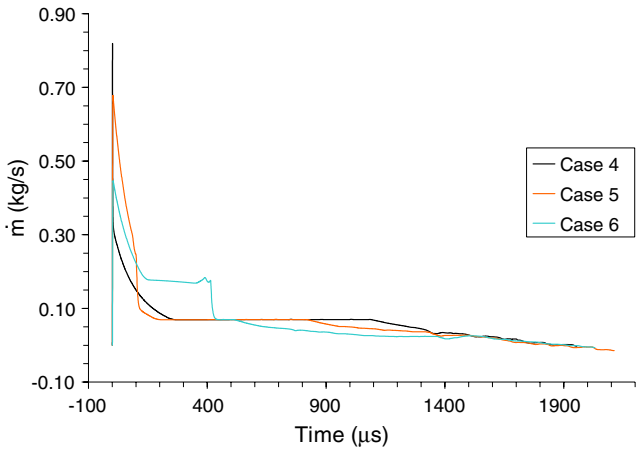

Fig. 7 Mass flow rate (kg/s) through the tube exit plane. $t = 0$ corresponds to the time at which the blast exits the tube. Cases 4–6

by a quasi-steady period of constant mass and energy delivery rate independent of the amount of reactants in the tube.

Figure 8 exhibits the flow rate of enthalpy for case 4, calculated at four different locations, namely, at the tube exit, and at one, two, and three tube diameters downstream of the tube exit (see Fig. 2). The same has been done for the mass flow rate as shown in Fig. 9. Figure 8 and 9 demonstrate the transient behavior of the exterior energy and mass delivery. The initial energy and mass delivery decays in a nonlinear manner. This is expected since the blast wave expands on the order of its radius squared over time (Ref 19).

An important performance parameter of a PDTS device is the fraction of powder delivered to the substrate target. It is obvious from the previous discussion that the combustion products (and powder) radially diverge as they exit the combustion tube. To quantify the performance of each case, the total mass delivered at each flow monitor was found by numerically integrating under each monitors flow rate versus time curve. The total mass delivered per cycle at each monitor is presented in Table 2 in nondimensional form. Here, a cycle is defined as the time between the blast wave exiting the PDTS tube and the start of flow reversal. All values are presented as a nondimensional fraction of the mass in the PDTS tube before firing, and can be viewed as a performance metric. As demonstrated by Fig. 6 and 7, a typical firing consists of an initial transient blast followed by a period of quasi-steady venting of the combustion products. The second

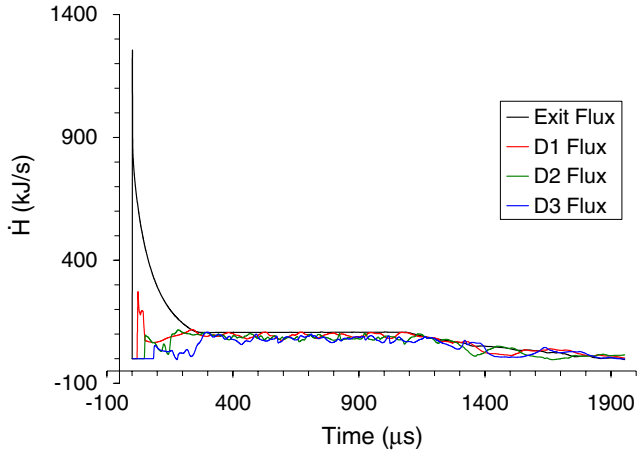

Fig. 8 Flow rate of enthalpy (kJ/s) for case 4, calculated at four different locations, namely, at the tube exit, and at one, two, and three tube diameters a head of the tube exit

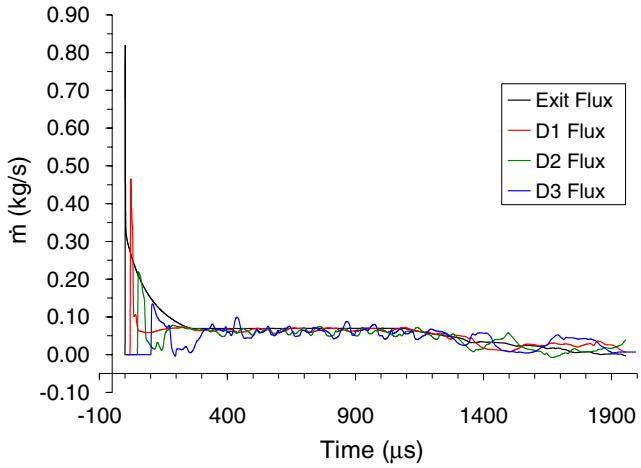

Fig. 9 Mass flow rate (kg/s) for case 4, calculated at four different locations, namely, at the tube exit, and at one, two, and three tube diameters a head of the tube exit

column in Table 3 shows the estimated time window of the quasi-steady jet which is qualitatively inferred from the mass-flow graphs. Columns 4-7 present, in dimensionless form, the fraction of available mass that crosses each location during the specified window of time. The peculiar, but outstanding, performance of D2 for cases 1-3 can be seen throughout Table 2 and 3.

While the quasi-steady jet gives a consistent delivery, the amount of mass delivered is lower than the mass delivered throughout the duration of the spray. The quasi-steady jet accounts for nearly 27% of the available mass for cases 1 and 4. However, the delivery of mass to the first target location (D1) during the quasi-steady period for the filled tube cases account for nearly 40% of the total mass delivered to that location. This relation improves as the distance increases from the tube exit. Cases 3 and 6

Table 2 Nondimensional fraction of mass delivered per cycle

			Flow monitors		
Case	Available mass	Exit mass fraction	D1 mass fraction	D2 mass fraction	D3 mass fraction
1	1.00	0.77	0.63	0.63	0.61
2	1.00	0.79	0.59	0.58	0.55
3	1.00	0.80	0.64	0.63	0.60
4	1.00	0.77	0.65	0.55	0.56
5	1.00	0.79	0.57	0.55	0.48
6	1.00	0.80	0.62	0.59	0.56

Table 3 Nondimensional fraction of mass delivered during the quasi-steady underexpanded jet

				Flow monitors		
Case	Time interval, μs ($t = 0$ blast exit)	Available mass	Exit mass fraction	D1 mass fraction	D2 mass fraction	D3 mass fraction
1	400-1000	1.00	0.27	0.26	0.25	0.25
2	300-800	1.00	0.21	0.21	0.21	0.20
3	200-300	1.00	0.10	0.09	0.09	0.09
4	400-1000	1.00	0.27	0.25	0.23	0.24
5	300-800	1.00	0.21	0.20	0.19	0.19
6	200-300	1.00	0.10	0.10	0.09	0.04

quasi-steady jets deliver much less mass because in these cases the steady jet is shorter in duration. Another conclusion is that cases 1 and 4 seem to be the least efficient. Cases 2, 3 and cases 5, 6 are much closer to each other for efficiency. The linear nature of the quasi-steady jet in the efficiency graphs indicates the predictable behavior of the jet during this time period. All cases leave some mass inside the tube. The cases leave almost 20-30% of the initial mass available in the tube. This is irrespective of the tube diameter.

6. Conclusions

Six cases representing tube diameters of 10 and 20 mm with three different amounts of fuel are studied in a 0.5-m long tube. Detonation is initiated in a mixture of 15.9% H_2 (by volume) in air. The combustion products in the tube are exhausted to a reservoir. The resulting blast wave and jet are studied until the instant in time when the flow reverses at the tube exit. Flow rates of enthalpy and the mass are recorded at the tube exit and at three potential axial target locations for all cases. Flow at the representative target locations and at the tube exit is monitored by numerical flow monitors.

Results obtained in this study indicate that there exists a quasi-steady jet in all six cases. During its existence, the quasi-steady jet is efficient and predictable in delivery of energy and mass from the tube exit to the flow monitors. This quasi-steady period is largest for the filled tube cases.

The quasi-steady jet represents nearly 40% of both the energy and mass that is delivered through the exterior flow monitors for the filled tube cases. Much of the initial energy and mass delivered avoids the flow monitors on the centerline. This is found to be related to the evolution of the jet behind the blast wave where energy is lost in expansion and vorticity production. It is also found that nearly 11-18% of energy and 20-23% of mass remains in the tube after flow reversal.

Although powder is not modeled in this study, the understanding of the performance of the gas by itself is shown to be informative. This type of study gives insight to the capability of the flow to deliver mass and energy. This capability can be used as a baseline for useful comparisons for mass and energy efficiency.

References

1. J.R. Fincke, W.D. Swank, R.L. Bewley, D.C. Haggard, M. Gevelber, and D. Wroblewski, Diagnostics and Control in the Thermal Spray Process, *Surf. Coat. Technol.*, 2001, **146-147**, p 537-543
2. H. Assadi, F. Gärtner, T. Stoltenhoff, and H. Kreye, Bonding Mechanism in Cold Gas Spraying, *Acta Mater.*, 2003, **51**, p 4379-4394
3. T. Stoltenhoff, H. Kreye, and H.J. Richter, An Analysis of the Cold Spray Process and Its Coatings, *J. Therm. Spray Technol.*, 2001, **11**, p 542-550
4. K.M., Ramadan, ''A Computational Study of Pulsed Detonation Thermal Spraying,'' PhD thesis, Department of Mechanical Engineering, The University of Iowa, 2002
5. P Saravanan, V. Selvarajan, D.S. Rao, S.V. Joshi, and G. Sundararajan, Influence of Process Variables on the Quality of Detonation Gun Sprayed Alumina Coatings, *Surf. Coat. Technol.*, 2000, **123**, p 44-54
6. R. Ishii, H. Fujimoto, N. Hatta, and Y. Umeda, Experimental and Numerical Analysis of Circular Pulse Jets, *J. Fluid Mech.*, 1999, **392**, p 129-153
7. K. Hsu and A. Jemcov, ''Numerical Investigation of Detonation in Premixed Hydrogen-Air Mixture: Assessment of Simplified Chemical Mechanisms,'' *Technical Report AIAA-2000-2478 Presented at the Fluids 2000 Conference and Exhibit*, June 19-22, 2000 (Denver, CO), 2000
8. A.K. Varma, A.U. Chatwani, and F.V. Bracco, Studies of Premixed Laminar Hydrogen-Air Flames Using Elementary and Global Kinetics Models, *Combust. Flame*, 1986, **64**, p 233-236
9. J.D. Anderson, Modern Compressible Flow: With Historical Perspective, 3rd ed., McGraw-Hill, New York, 2003
10. P.B. Butler and R.G. Schmitt: ''RGEQUIL,'' 1995, The University of Iowa
11. A.P. Raghupathy, U. Ghia, and K. Ghia, ''A Comparative Study of Chemical Mechanisms in the Simulation of One-Dimensional Detonation,'' *Paper Presented at the 42nd AIAA/ASME/SAE/ASEE Joint Propulsion Conference and Exhibit*, July 9-12, 2006 (Sacramento, CA), 2006
12. M.-S. Liou and C.J Steffen, A New Flux Splitting Scheme, *J. Comput. Phys.*, 1993, **107**, p 23-39
13. M.-S. Liou, A Sequel to AUSM: AUSM+, *J. Comput. Phys.*, 1996, **129**, p 364-382
14. M. Dumbser, J.-M. Moschetta, and J. Gressier, A Matrix Stability Analysis of the Carbuncle Phenomenon, *J. Comput. Phys.*, 2004, **197**, p 647-670
15. J.J. Quirk, A Contribution to the Great Riemann Solver Debate, *Intl. J. Numer. Meth. Fluid*, 1994, **18**, p 555-574
16. S.R. Chakravarthy and S. Osher, '' A New Class of High Accuracy TVD Schemes for Hyperbolic Conservation Laws,'' *AIAA Paper*, 1985, 85-0363
17. J.E. Cannon, ''Thermal Efficiency Delivery of a Detonation Induced Pulse Jet,'' M.S. thesis, Department of Mechanical Engineering, The University of Iowa, 2007
18. K.K. Kuo, Principles of Combustion, 2nd ed., John Wiley & Sons, New Jersey, 2005
19. S.-C. Lin, Cylindrical Shock Waves Produced by Instantaneous Energy Release, *J. Appl. Phys.*, 1954, **25**, p 54-57